Silver Nanoclusters

International Edition: DOI: 10.1002/anie.201809469
German Edition: DOI: 10.1002/ange.201809469

Camouflaging Structural Diversity: Co-crystallization of Two Different Nanoparticles Having Different Cores But the Same Shell

*Mohammad Bodiuzzaman[+], Atanu Ghosh[+], Korath Shivan Sugi, Abhijit Nag, Esma Khatun, Babu Varghese, Ganesan Paramasivam, Sudhadevi Antharjanam, Ganapati Natarajan, and Thalappil Pradeep**

Abstract: *Two ligand-protected nanoscale silver moieties, $[Ag_{46}(SPhMe_2)_{24}(PPh_3)_8](NO_3)_2$ and $[Ag_{40}(SPhMe_2)_{24}(PPh_3)_8](NO_3)_2$ (abbreviated as Ag_{46} and Ag_{40}, respectively) with almost the same shell but different cores were synthesized simultaneously. As their external structures are identical, the clusters were not distinguishable and become co-crystallized. The occupancy of each cluster was 50%. The outer shell of both is composed of $Ag_{32}S_{24}P_8$, which is reminiscent of fullerenes, and it encapsulates a well-studied core, Ag_{14} and a completely new core, Ag_8, which correspond to a face-centered cube and a simple cube, respectively, resulting in the Ag_{46} and Ag_{40} clusters. The presence of two entities (Ag_{40} and Ag_{46} clusters) in a single crystal and their molecular formulae were confirmed by detailed electrospray ionization mass spectrometry. The optical spectrum of the mixture showed unique features which were in good agreement with the results from time-dependent density functional theory (TD-DFT).*

Many molecular clusters of noble metals have been crystallized in the recent past.[1–17] All of them can be understood by the divide-and-protect formalism in which metal cores are protected by a composite shell, often formed of staple motifs.[18] The molecular architecture providing structural rigidity is also associated with a closed-shell electronic structure, making such cluster systems stable.[19,20] A unique possibility in such structures is the existence of a common outer shell with varied inner cores. Nucleation of different cores in the reaction vessel can consequently create such varied structures composed of different cores and same shell simultaneously. Their co-crystallization can lead to new materials.

In this work, we present the complete characterization of such a co-crystal. Upon resolving the structure of such a disordered co-crystal, we obtained the formulae of component clusters as $[Ag_{46}(SPhMe_2)_{24}(PPh_3)_8](NO_3)_2$ and $[Ag_{40}(SPhMe_2)_{24}(PPh_3)_8](NO_3)_2$, also represented as Ag_{46} and Ag_{40}, respectively, with 1:1 occupancy in the crystal. Single-crystal X-ray diffraction (SCXRD) shows that the clusters have an almost identical outer shell ($Ag_{32}S_{24}P_8$) with variation only in the inner core (Ag_{14} and Ag_8). Unlike Ag_{14}, the Ag_8 inner core was not observed before. Existence of the two new clusters in a single crystal and their molecular formulae were confirmed by electrospray ionization mass spectrometry (ESI MS). This identification can open up new avenues of tailoring and elucidating the properties of such well-defined composite materials. The Ag_{46} and Ag_{40} units with their ligands are referred to as **I** and **II** in the subsequent discussion.

A mixture of **I** and **II** clusters was synthesized by a ligand-exchange-induced structure transformation (LEIST) process. In this process, $[Ag_{18}H_{16}(PPh_3)_{10}]^{2+}$ was used as the precursor material and the ligand exchange reaction was performed with 2,4-dimethylbenzenethiol ($SPhMe_2$) (see the Experimental Section in the Supporting Information). The precursor material was synthesized following a method reported by the Bakr group (Figure S1).[21] Single crystals were grown by layering hexane onto a dichloromethane solution of pure nanoclusters at 4 °C. Dark black crystals were obtained over a period of 5–7 days. A mixture of as-synthesized clusters crystallizes in a C-centered monoclinic system with space group *C*2/*m*.[22] From the SCXRD analysis (see the Supporting Information for detailed analysis), it could be unambiguously inferred that there are two types of molecules in the lattice which are nearly isostructural but differing by six silver atoms. In other words, the two molecules are isodimensional and one can replace the position of the other. The total structures of **I** (Figure 1 A,C) and **II** (Figure 1 B,D) are shown in ball-and-stick and space-filling models, which reveal their isodimensionality. Six sites of **[I]**$(NO_3)_2$ are vacant in **[II]**$(NO_3)_2$. Owing to their nearly identical outer shell, they are not able to distinguish themselves and crystallize together. Therefore, the six-atom difference does not come into the picture during the growth of the crystals and both the clusters are nucleated in equal proportion in a single crystal. We believe that this arises because of their equal concentration in the solution. A dissection of **I** and **II** was conducted based on the connectivity of silver atoms to ligands to get the inner cores (the metal structures that are not connected to ligands). The structures of inner cores, Ag_8 (in **II**) and Ag_{14} (in **I**) are presented in Figure 2 A,D, respectively. Both the cores are encapsulated by the $Ag_{32}S_{24}P_8$ shell (Figure 2 B,E), which is reminiscent of fullerenes. Total structures of $[Ag_{40}S_{24}P_8]$ and

[*] M. Bodiuzzaman,[+] Dr. A. Ghosh,[+] K. S. Sugi, A. Nag, E. Khatun, Dr. G. Paramasivam, Dr. G. Natarajan, Prof. T. Pradeep
Department of Chemistry, DST Unit of Nanoscience (DST UNS) and Thematic Unit of Excellence (TUE)
Indian Institute of Technology Madras
Chennai 600036 (India)
E-mail: pradeep@iitm.ac.in
Dr. B. Varghese, Dr. S. Antharjanam
Sophisticated Analytical Instruments Facility
Indian Institute of Technology Madras
Chennai 600036 (India)
[+] These authors contributed equally to this work.
Supporting information and the ORCID identification number(s) for the author(s) of this article can be found under: https://doi.org/10.1002/anie.201809469.

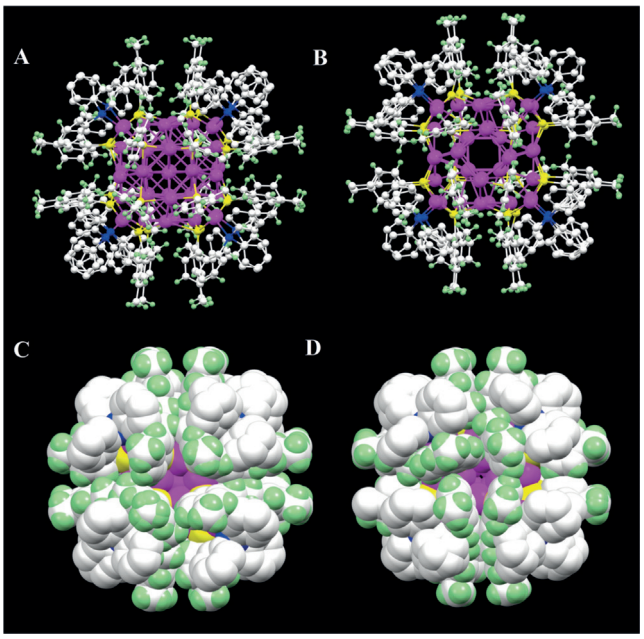

Figure 1. A),B) Ball-and-stick models of Ag_{46} and $Ag_{40,}$ respectively. Note the difference in the center of the cluster. C),D) The same in space-filling model (hydrogens of triphenylphosphines are not fixed). It is clear that the outer shells of the clusters are nearly identical. Counterions are not shown. C white, Ag magenta, S yellow, P blue, H light green.

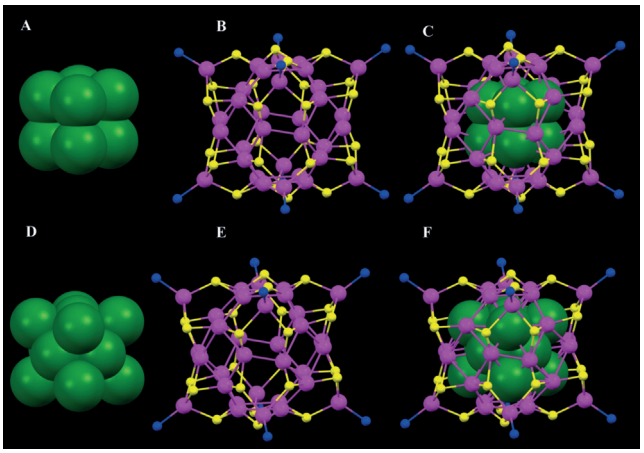

Figure 2. A),D) Ag_8 and Ag_{14} inner-core structures of Ag_{40} and Ag_{46}, respectively. The inner cores Ag_8 and Ag_{14} correspond to simple cubic and face-centered cubic structures, respectively. B),E) $Ag_{32}S_{24}P_8$ shell; that is, the structures of the clusters without metal cores. C),F) The structures of $[Ag_{40}S_{24}P_8]$ and $[Ag_{46}S_{24}P_8]$, respectively. Carbon and hydrogen atoms are omitted for clarity. Ag green and magenta, S yellow, P blue.

$[Ag_{46}S_{24}P_8]$ are shown in Figure 2 C,F, respectively (carbon and hydrogen atoms are omitted here). The core and shell structures presented for these two clusters (Figure 2) can be viewed in different ways in the context of known structures. A compendium of such known structures is presented in the Supporting Information, Table S1, which brings out unique aspects of the new structures. The first unique aspect is the completely new kind of core Ag_8 (in **II**) and the well-studied core Ag_{14} (in **I**);[23–25] they correspond to perfect simple cubic and face-centered cubic structures, respectively. The face-centered cubic structure (Ag_{14}) can also be visualized as octacapped octahedron, $Ag_6@Ag_8$ (Figure S2A–C). Here, the $Ag_{octahedron}$–Ag_{cube} distance is 2.70 Å, which indicates the strong interaction between the core atoms. The surface of the octahedral Ag_6 (Figure S2B) inner core is surrounded by eight equilateral triangle-shaped planes, a fragment of bulk FCC metals.[24] The average Ag–Ag bond distance in octahedral Ag_6 is 2.88 Å, which is almost same as that in bulk (2.89 Å).[26] Around the octahedral Ag_6 core, there are eight Ag atoms, which make a cube (Figure S2A). The average distance between the corners of the cube is 3.8 Å, which is much shorter than that of other reported FCC structures (the same distance is about 4.2 Å).[23,24] The surfaces of the Ag_8 cube are covered by six square-shaped {100} (Figure S3A) facets. Along with this, other facets like rectangular-shaped {110} (Figure S3B) and equilateral triangle-shaped {111} (Figure S3C) are observed. All these facets are shown in ball-and-stick model (Figure S3). In case of **II**, the inner core atoms of the simple cube are bonded very strongly with average Ag–Ag distances of 2.68 Å, which is much shorter than in bulk silver.[26]

The formation of a common shell, $Ag_{32}S_{24}P_8$ (Figure S4C) can be described as composed of Ag_{24} (Figure S4B) outer core covered by eight units of Ag^I-thiolate-phosphine complex (AgS_3P) (Figure S4A). The Ag_{24} outer core can be viewed as it is composed of eight shared hexagonal faces (Figure S4D). AgS_3P units are sitting on the faces of eight hexagons of Ag_{24} outer core to form the framework, $Ag_{32}S_{24}P_8$ (Figure S4F). Each sulfur of AgS_3P bridges the two adjacent silver atoms of a hexagon (Figure S4F). Here the average Ag–Ag distance within the hexagons is 2.92 Å. Another way of looking into the outer core (Ag_{24}) is in terms of six square faces (Figure S5A). The faces are shown in different colors (Figure S5A). Average Ag–Ag distance in the square face is 3.0 Å and square faces are connected by a bond length of 2.86 Å. In this ligand shell, average Ag–S and Ag–P distances are 2.64 Å and 2.45 Å, respectively. It is worth noting that all the Ag–Ag distances in the outer Ag_{24} core are exactly same in both the clusters. A summary of Ag–Ag distances is presented in the Supporting Information, Table S2. The bonding between the inner core and outer core are not same in **I** and **II** clusters. In **I** the squares of Ag_{24} outer core are connected to the six silver atoms of octahedral Ag_6 (Figure S5B), forming a six square-pyramid-like architecture (Figure S5C). One such square-pyramid is shown in wireframe model (Figure S5D). In this architecture, Ag–Ag distances between silver atoms on the apex and the square faces are 3.0 Å. Such a square-pyramid-like architecture is not observed in the **II** cluster owing to the absence of an octahedral (Ag_6) inner core. The further differences in bonding between the outer (Ag_{24}) and inner cores in **I** and **II** clusters will be explained later.

A packing diagram of both the clusters is shown in the Supporting Information, Figure S6. Both the clusters are packed in an identical fashion in all the axes and the contribution of each component cluster is 50%. **II** is organized into centered rectangular (Figure S6A) and rectangular (Figure S6C) two-dimensional (2D) lattices along

the z and x direction, respectively. Similar packing is observed for **I** (Figure S6B,D; along the z and x direction, respectively). The crystal structure resolved nitrate as the counter ion and the packing structure clearly indicates the location of two counter ions per cluster (Figure S7). However, the packing is identical for both the molecules (Figure S6), the stacking of silver atoms in their kernels is different. The term kernel refers to the combined unit of outer and inner cores. The construction of Ag_{32} (in **II**) and Ag_{38} (in **I**) kernels are shown in Figure S8. The Ag_{24} outer core (Figure S8A) encapsulates Ag_8 inner core to form Ag_{32} kernel (Figure S8B). Similarly, Ag_{38} kernel (Figure S8D) is formed by the combination of Ag_{24} outer core and Ag_{14} inner core. In Ag_{32} kernel (in **II**), atoms of the Ag_8 core take upward and downward positions of the hexagonal faces of Ag_{24} outer core (Figure S8B), and thus the eight silver atoms are not in the same plane of hexagons (Figure S8B,C). In the Ag_{38} kernel (in **I**), eight silver atoms that are at the corners of the face-centered cube occupy the center position of the hexagon of the Ag_{24} outer core (Figure S8D). Here it is important to note that all the atoms of the hexagon are coordinated to its centered silver atom in Ag_{38} kernel (in **I**; Figure S8E) but in Ag_{32} (in **II**) only a few atoms of the hexagon are connected to its upward and downward positioned silver atom (Figure S8C). Stacking of the atoms in the Ag_{38} and Ag_{32} kernels are shown in Figure 3. The Ag_{38} kernel (in **I**) exhibits ABC stacking (Figure 3 A–C) owing to the in-plane arrangements of the atoms. The stacking planes are shown with three different color arrows in Figure 3 A. Such stacking is not observed for Ag_{32} kernel (in **II**) as the atoms of inner core (Ag_8) take upward and downward positions of the hexagonal faces of Ag_{24} outer core (Figure 3 D–F). Space-filling model for both the kernels, Ag_{38} and Ag_{32} are presented in Figure 3 C and F, respectively. Stacking is consistent in other rotations also as shown in Figure 3 B and E for Ag_{38} and Ag_{32} kernels, respectively. The structure of Ag_{38} kernel can also be viewed as an inner Ag_6 octahedron, surrounded by a truncated-octahedral shell of Ag_{32} (Figure S9A), which is having close resemble to the predicted structure of $Au_{38}(SR)_{24}$.[27] The truncated octahedron shell is shown in wireframe model (Figure S9B) and the Ag_6 octahedron is presented in space-filling model (Figure S9C).

ESI MS shows the coexistence of those two entities (**I** and **II**) in a single crystal. For this, a single crystal was dissolved in methanol and mass spectral measurement was performed. Sample preparation and instrumental conditions are given in Supporting Information. Full range mass spectrum shows three major peaks at m/z 3235.75, 4853.5, and 5176.25 in positive-ion mode (Figure 4 A). Peaks at m/z 5176.25 and 4853.50 are expanded in the Supporting Information, Figures S10A,B. They show the characteristic peak separation of m/z 0.5, which confirm their 2+ charge state. Similarly, the separation between peaks centered at m/z 3235.75 is 0.33 which confirms the 3+ charge state (Figure S10C). The peaks at m/z 4853.5 and 3235.75 are assigned as $\mathbf{II}^{2+}$ and $\mathbf{II}^{3+}$, respectively. Comparison of isotopic distributions of experimental (black trace) and simulated (red trace) confirm the composition (Figure 4A1,A2). Existence of two charge states in the mass spectrum was also reported previously for the $[Ag_{44}(p\text{-MBA})_{30}]^{4-}$ (p-MBA: 4-mercaptobenzoic acid) cluster.[8] Seemingly, population of Ag_{40}^{2+} is major in the solution phase and Ag_{40}^{3+} might be present in the gas phase. Similarly, the peak at m/z 5176.25 is assigned as $\mathbf{I}^{2+}$. The experimental (black trace) and simulated (red trace) isotopic distributions

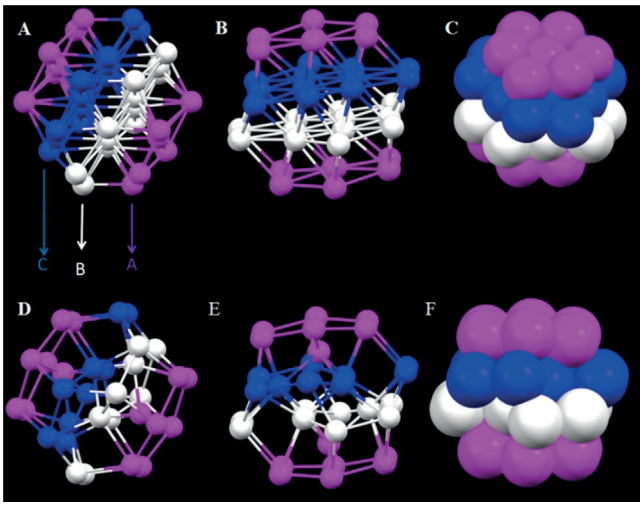

Figure 3. A),B) The structure of Ag_{38} kernel in two different rotations along the z axis (removing all the carbons, hydrogens, and eight AgS_3P units from total structure of Ag_{46}) in ball-and-stick model. D),E) The structure of Ag_{32} kernel in two different rotations along the z axis (removing all the carbons, hydrogens, and eight AgS_3P units from total structure of Ag_{40}) in ball-and-stick model. C),F) Space-filling model of (B) and (E), respectively. The ABC stacking planes are shown by three different color arrows in Ag_{38} kernel (in Ag_{46}). Such stacking is not observed for Ag_{32} kernel (in Ag_{40}). All atoms shown are silver.

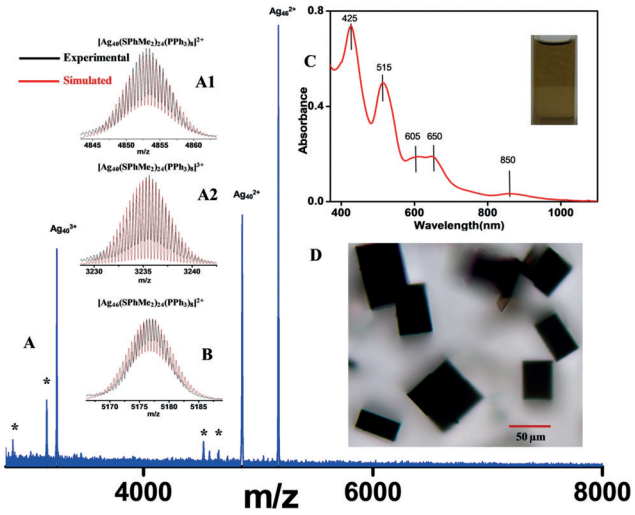

Figure 4. A) Full-range ESI MS of a methanol solution of crystals in positive ion mode. The major peaks are due to Ag_{40}^{2+}, Ag_{40}^{3+} and Ag_{46}^{2+}. Peaks labeled with an asterisk (*) correspond to PPh_3 losses from these ions. Insets A1),A2) Comparison of experimental (black trace) and simulated (red trace) isotopic distributions of Ag_{40}^{2+} and Ag_{40}^{3+}, respectively. B) The experimental (black) and simulated (red) isotopic distributions of Ag_{46}^{2+} are compared. C) UV/Vis absorption spectrum of a solution of crystals in dichloromethane. Inset: Visible light photograph of the cluster solution. D) Optical image of the crystals.

are compared in Figure 4B, which supports the assigned composition. The above observations prove the presence of two species, **I** and **II** in a single crystal. However, one may think whether **II** is formed from **I** by decomposition in the gas phase. To probe this possibility, we performed collision-induced dissociation (CID) experiments on $\mathbf{I}^{2+}$, which resulted in systematic triphenylphosphine losses as expected owing to the weaker interaction of the secondary ligands,[6,28] yielding **I**-$(PPh_3)_8^{2+}$; however no **II** in any charge state was detected (Figure S11). CID mass spectra of **I** and **II** revealed a maximum loss of eight triphenylphosphines in **I** (Figure S12A) and **II** (Figure S12B) clusters, which supports the number of triphenylphosphines present in the cluster formulae. Hence, it is shown that in the gas phase there is no fragmentation of **I** to create **II**, but the possibility of formation of **II** by oxidation of **I** in the solution phase exists. To rule out this possibility, the solution of a mixture of **I** and **II** was heated and stirred in methanol at 50 °C and products were analyzed by UV/Vis and ESI MS as a function of time. Time-dependent UV/Vis spectra showed no significant change with times up to 8 h, only a change in the absorbance was observed. After 8 h, the features of UV/Vis spectra started to disappear, seemingly due to the decomposition of the cluster (Figure S13B). Time-dependent ESI MS exhibited presence of the species, **I** and **II** and no signature of conversion was observed as relative intensities of **I** and **II** were the same. After 8 h, the intensities in the ESI MS started to decrease and the peaks disappeared after 12 h, which confirmed the decomposition of the clusters (Figure S13A). It confirmed that **II** is not the oxidation product of **I**. The UV/Vis spectrum of a mixture of **I** and **II** was measured by dissolving crystals in DCM, which exhibits molecule-like optical absorption that displays three prominent peaks (at 425, 515, and 650 nm) and two shoulder peaks at 605 and 850 nm (Figure 4C). The inset shows a visible-light photograph of the cluster solution. Some of the spectral features are comparable to the clusters, $[Ag_{25}(SPhMe_2)_{18}]^-$, $[Ag_{44}(FTP)_{30}]^{4-}$ (FTP: 4-fluorothiophenol) and $[Ag_{67}(SPhMe_2)_{32}(PPh_3)_8]^{3+}$, but the overall spectrum is very different (Figures S14,S15).[4–6] An optical image of the single crystals is shown in Figure 4D.

Thin-layer chromatography (TLC) and high-performance liquid chromatography (HPLC)-based procedures to separate the components of the co-crystals were unsuccessful. We had introduced TLC as a separation technique for gold clusters.[29] Seemingly the high charge on the clusters resulted in stronger interactions with the stationary phase and the components were not eluted. In HPLC, the clusters were decomposed after passing through the column. Although HPLC separation is well established for gold clusters, no separation of silver clusters has been accomplished till now and therefore this inability is not surprising. However, to explore the optical properties of individual clusters, we have separately synthesized and characterized both the component clusters. Compound **II** was synthesized with almost complete absence of **I** (Figure S16) by changing the synthetic conditions, while **I** was made by using an isomeric thiol (2,4-$SPhMe_2$ was changed to 2,5-$SPhMe_2$; see the Supporting Information). ESI MS and UV/Vis spectra of pure Ag_{46} are presented in the Supporting Information, Figure S17A,C, respectively. Comparison of experimental isotopic distributions with the simulated one confirms the cluster formula (Figure S17B). One of the components (Ag_{46}) has been crystallized and it is having the same structure (Figure S18A,C) as present in the co-crystal (Figure S18B,D). Crystal analysis of 2,5-$SPhMe_2$ protected Ag_{46} is given in the Supporting Information. Unfortunately, we could not grow the single crystal of **II** alone owing to its instability in pure form. The higher stability of **I** can be seen from a time-dependent UV/Vis study. Solutions of Ag_{40} and Ag_{46} were heated and stirred in methanol at 50 °C and products were analyzed by UV/Vis spectroscopy (Figure S19). UV/Vis spectra revealed the disappearance of highly structured features of **II** after 1.5 h (Figure S19A). In the case of **I**, the spectral features and absorbance were the same up to 3 h, change in absorbance was seen only afterwards (Figure S19B). This observation clearly indicates that Ag_{46} is indeed more stable. UV/Vis-NIR spectra of the individual clusters are shown in the Supporting Information, Figure S20 and **II** exhibit an absorption in the NIR region (1279 nm) that is absent in **I** (Figure S20). A unique possibility of mixing the two clusters in different ratios in solution may tune their ratios in the co-crystal and this can open up a new direction in cluster chemistry. However, it may be noted that the mixing ratio may not be the occupancy ratio in the crystal, which is decided by minimum potential energy considerations.

To estimate the HOMO–LUMO gap of **I** and **II**, differential pulse voltammetry (DPV) was performed. DPV results show several peaks in positive and negative potential regions which are assigned as oxidation and reduction peaks, respectively (Figure S21). The HOMO–LUMO gaps of **I** and **II** were determined to be about 1.30 eV and 0.92 eV, respectively (Figure S21). The analysis and experimental details are described in Supporting Information.

The electronic structures of **II** and **I** were analyzed by using the model clusters with reduced ligands, $[Ag_{40}(SCH_3)_{24}(P(CH_3)_3)_8]$ (Figure S22A) and $[Ag_{46}(SCH_3)_{24}(P(CH_3)_3)_8]$ (Figure S22B), respectively. Here the coordinates of Ag, S, and P atoms were taken from crystal structures and were kept fixed, but C and H atoms were allowed to relax. The electronic structure and optical absorption of the clusters were investigated using density functional theory (DFT) and time-dependent density functional theory (TDDFT) using the projector augmented wave (PAW) method as implemented in GPAW.[30] The optical absorption spectra were calculated using linear response TDDFT.[31] The theoretical spectrum (black trace) of a 1:1 mixture of both the clusters, constructed from the predictions of individual clusters (Figure S23) is compared with the experimental spectrum (red trace) in Figure 5. The match is particularly good in the higher wavelength region. This further proves the existence of both the structures together in the crystal. Various electronic transitions (Table S3) and the charge density distribution of the frontier orbitals suggest the involvement of most of the atoms. Molecular orbital (MO) transitions to the optical gap of $[Ag_{46}(SCH_3)_{24}(P(CH_3)_3)_8]^{2+}$ and $[Ag_{40}(SCH_3)_{24}(P(CH_3)_3)_8]^{2+}$ are presented in the Supporting Information, Figures S24 and S25, respectively. The structure of Ag_{40}^{3+} cluster was also optimized to calculate the optical absorption

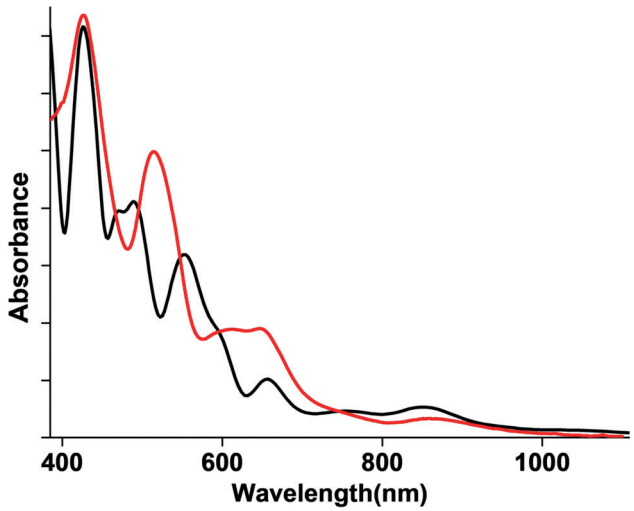

Figure 5. Black trace corresponds to the theoretical spectrum of a 1:1 mixture of both the clusters ($[Ag_{46}(SCH_3)_{24}(P(CH_3)_3)_8]$ and $[Ag_{40}(SCH_3)_{24}(P(CH_3)_3)_8]$) constructed from the theoretical prediction. Red trace indicates the experimental spectrum of mixture of both the clusters.

spectrum and it is compared with that of Ag_{40}^{2+} cluster in the Supporting Information, Figure S26. In general, the spectrum of Ag_{40}^{3+} cluster is similar to that of the Ag_{40}^{2+} cluster. To understand the origin of the optical transitions having the highest oscillator strength (f) of $\mathbf{I}^{2+}$ and $\mathbf{II}^{2+}$, density of states (DOS) were calculated and they are plotted in the Supporting Information, Figure S27 and S28. The transitions taking place at 410.03 nm ($f = 0.373$) and 441.49 nm ($f = 0.225$) for $\mathbf{I}^{2+}$ and $\mathbf{II}^{2+}$ clusters, respectively are considered here. DOS calculations conclude that in the case of $\mathbf{I}^{2+}$ the major contributing MOs are HOMO−3 and LUMO + 8. These occupied MOs (as denoted by the dotted vertical lines in the Supporting Information, Figure S27 D) are mainly contributed by the 3p atomic orbitals (AOs) of sulfur, 5s, 5p AOs of silver atoms in shell regions, and 5s AOs of Ag atoms in the core, and the unoccupied MOs are formed by 5p AOs of shell silver atoms. In the case of $\mathbf{II}^{2+}$, the significant contribution to the transition is from HOMO−1 to LUMO + 11 and these two MOs (as denoted by the dotted vertical lines in the Supporting Information, Figure S27 B) are predominantly composed of 5s and 5p AOs of Ag atoms from the shell region of the cluster, respectively. Hence, these optical absorption transitions exhibit a similar characteristic for both **I** and **II** clusters. By using the widely used rule[19] to count the free electrons for $\mathbf{I}^{2+}$ and $\mathbf{II}^{2+}$ in the metal core, we get 20 and 14 free electrons in them, respectively. Both the clusters could be viewed as superatomic with 20 and 14 electrons distributed in superatomic orbitals as shown in the Supporting Information, Figure S29 and S31, respectively. The isosufaces of superatomic orbitals of both the clusters are plotted in the Supporting Information, Figures S30 and S32.

In conclusion, we present the possibility of crystallization of structurally similar clusters together leading to new nanocrystal solids. A new category of such crystals is those composed of different cores with the same shell. It is surprising that Ag_8 and Ag_{14} inner cores are nucleated simultaneously in solution with equal probability. The mechanism of such cluster growth and their encapsulation in shells require additional studies. This observation suggests the possibility of the coexistence of diverse clusters and their co-crystallization. Such nanocluster co-crystals, similar to superlattices will be a way forward to realize cluster assembled materials with new properties. Along with these, it is worthy to mention the observation of a rigid polymeric ligand shell which remains unaltered after removing or adding six silver atoms.

Acknowledgements

We thank Department of Science and Technology for supporting our research project. We thank the Sophisticated Analytical Instruments Facility, Indian Institute of Technology Madras for SCXRD data collection. M.B., A.G. and K.S.S. thank U.G.C. for their research fellowships. A.N. and E.K. thank IITM for their fellowships. G.P. thanks IITM for an Institute Postdoctoral fellowship. We thank Sourav Kanti Jana for his inputs in performing electrochemical experiments.

Conflict of interest

The authors declare no conflict of interest.

Keywords: Ag_{40} · Ag_{46} · co-crystals · nanoclusters

How to cite: *Angew. Chem. Int. Ed.* **2019**, *58*, 189–194
Angew. Chem. **2019**, *131*, 195–200

[1] I. Chakraborty, T. Pradeep, *Chem. Rev.* **2017**, *117*, 8208.
[2] R. Jin, C. Zeng, M. Zhou, Y. Chen, *Chem. Rev.* **2016**, *116*, 10346.
[3] L. G. AbdulHalim, M. S. Bootharaju, Q. Tang, S. Del Gobbo, R. G. AbdulHalim, M. Eddaoudi, D.-e. Jiang, O. M. Bakr, *J. Am. Chem. Soc.* **2015**, *137*, 11970.
[4] C. P. Joshi, M. S. Bootharaju, M. J. Alhilaly, O. M. Bakr, *J. Am. Chem. Soc.* **2015**, *137*, 11578.
[5] H. Yang, Y. Wang, H. Huang, L. Gell, L. Lehtovaara, S. Malola, H. Häkkinen, N. Zheng, *Nat. Commun.* **2013**, *4*, 2422.
[6] M. J. Alhilaly, M. S. Bootharaju, C. P. Joshi, T. M. Besong, A.-H. Emwas, R. Juarez-Mosqueda, S. Kaappa, S. Malola, K. Adil, A. Shkurenko, H. Häkkinen, M. Eddaoudi, O. M. Bakr, *J. Am. Chem. Soc.* **2016**, *138*, 14727.
[7] R. S. Dhayal, J.-H. Liao, Y.-C. Liu, M.-H. Chiang, S. Kahlal, J.-Y. Saillard, C. W. Liu, *Angew. Chem. Int. Ed.* **2015**, *54*, 3702; *Angew.Chem.* **2015**, *127*, 3773.
[8] A. Desireddy, B. E. Conn, J. Guo, B. Yoon, R. N. Barnett, B. M. Monahan, K. Kirschbaum, W. P. Griffith, R. L. Whetten, U. Landman, T. P. Bigioni, *Nature* **2013**, *501*, 399.
[9] M. W. Heaven, A. Dass, P. S. White, K. M. Holt, R. W. Murray, *J. Am. Chem. Soc.* **2008**, *130*, 3754.
[10] P. D. Jadzinsky, G. Calero, C. J. Ackerson, D. A. Bushnell, R. D. Kornberg, *Science* **2007**, *318*, 430.
[11] C. Zeng, H. Qian, T. Li, G. Li, N. L. Rosi, B. Yoon, R. N. Barnett, R. L. Whetten, U. Landman, R. Jin, *Angew. Chem. Int. Ed.* **2012**, *51*, 13114; *Angew.Chem.* **2012**, *124*, 13291.
[12] M. S. Bootharaju, C. P. Joshi, M. R. Parida, O. F. Mohammed, O. M. Bakr, *Angew. Chem. Int. Ed.* **2016**, *55*, 922; *Angew. Chem.* **2016**, *128*, 934.

[13] G. Soldan, M. A. Aljuhani, M. S. Bootharaju, L. G. AbdulHalim, M. R. Parida, A.-H. Emwas, O. F. Mohammed, O. M. Bakr, *Angew. Chem. Int. Ed.* **2016**, *55*, 5749; *Angew. Chem.* **2016**, *128*, 5843.
[14] C. Liu, T. Li, H. Abroshan, Z. Li, C. Zhang, H. J. Kim, G. Li, R. Jin, *Nat. Commun.* **2018**, *9*, 744.
[15] H. Yang, J. Yan, Y. Wang, G. Deng, H. Su, X. Zhao, C. Xu, B. K. Teo, N. Zheng, *J. Am. Chem. Soc.* **2017**, *139*, 16113.
[16] W. Du, S. Jin, L. Xiong, M. Chen, J. Zhang, X. Zou, Y. Pei, S. Wang, M. Zhu, *J. Am. Chem. Soc.* **2017**, *139*, 1618.
[17] L. Ren, P. Yuan, H. Su, S. Malola, S. Lin, Z. Tang, B. K. Teo, H. Häkkinen, L. Zheng, N. Zheng, *J. Am. Chem. Soc.* **2017**, *139*, 13288.
[18] H. Häkkinen, M. Walter, H. Grönbeck, *J. Phys. Chem. B* **2006**, *110*, 9927.
[19] M. Walter, J. Akola, O. Lopez-Acevedo, P. D. Jadzinsky, G. Calero, C. J. Ackerson, R. L. Whetten, H. Grönbeck, H. Häkkinen, *Proc. Natl. Acad. Sci. USA* **2008**, *105*, 9157.
[20] J. U. Reveles, S. N. Khanna, P. J. Roach, A. W. Castleman, *Proc. Natl. Acad. Sci. USA* **2006**, *103*, 18405.
[21] M. S. Bootharaju, R. Dey, L. E. Gevers, M. N. Hedhili, J.-M. Basset, O. M. Bakr, *J. Am. Chem. Soc.* **2016**, *138*, 13770.
[22] CCDC 1842077 contains the supplementary crystallographic data for this paper. These data are provided free of charge by The Cambridge Crystallographic Data Centre.
[23] H. Yang, J. Yan, Y. Wang, H. Su, L. Gell, X. Zhao, C. Xu, B. K. Teo, H. Häkkinen, N. Zheng, *J. Am. Chem. Soc.* **2017**, *139*, 31.
[24] S. Jin, S. Wang, Y. Song, M. Zhou, J. Zhong, J. Zhang, A. Xia, Y. Pei, M. Chen, P. Li, M. Zhu, *J. Am. Chem. Soc.* **2014**, *136*, 15559.
[25] H. Yang, J. Lei, B. Wu, Y. Wang, M. Zhou, A. Xia, L. Zheng, N. Zheng, *Chem. Commun.* **2013**, *49*, 300.
[26] R. Fournier, *J. Chem. Phys.* **2001**, *115*, 2165.
[27] H. Häkkinen, R. N. Barnett, U. Landman, *Phys. Rev. Lett.* **1999**, *82*, 3264.
[28] A. Ghosh, M. Bodiuzzaman, A. Nag, M. Jash, A. Baksi, T. Pradeep, *ACS Nano* **2017**, *11*, 11145.
[29] A. Ghosh, J. Hassinen, P. Pulkkinen, H. Tenhu, R. H. A. Ras, T. Pradeep, *Anal. Chem.* **2014**, *86*, 1218526.
[30] J. J. Mortensen, L. B. Hansen, K. W. Jacobsen, *Phys. Rev. B* **2005**, *71*, 035109.
[31] M. Walter, H. Hakkinen, L. Lehtovaara, M. Puska, J. Enkovaara, C. Rostgaard, J. J. Mortensen, *J. Chem. Phys.* **2008**, *128*, 244101.

Manuscript received: August 16, 2018
Revised manuscript received: October 14, 2018
Accepted manuscript online: November 8, 2018
Version of record online: November 25, 2018

